

A Hierarchically Tailored Wrinkled Three-Dimensional Foam for Enhanced Elastic Supercapacitor Electrodes

Syeon Jang, Hyeongho Min, Sung Beom Cho, Hyeon Woo Kim, Wonkyeong Son, Changsoon Choi, Sungwoo Chun,* and Changhyun Pang*



Cite This: *Nano Lett.* 2021, 21, 7079–7085



Read Online

ACCESS |

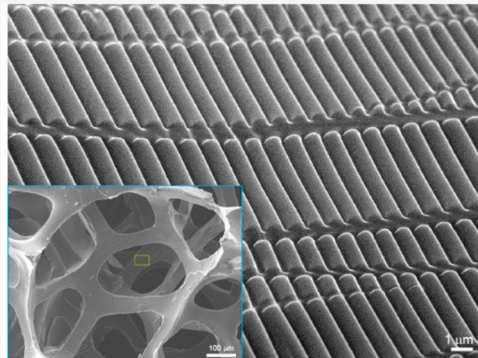
Metrics & More

Article Recommendations

Supporting Information

ABSTRACT: Recently, three-dimensional (3D) porous foams have been studied, but further improvement in nanoscale surface area and stretchability is required for electronic and energy applications. Herein, a general strategy is reported to form a tailored wrinkling structure on strut surfaces inside a 3D polydimethylsiloxane (PDMS) polymeric foam. Controlled wrinkles are created on the struts of 3D foam through an oxygen plasma treatment to form a bilayer surface of PDMS on uniaxially prestretched 3D PDMS foam, followed by relaxation. After plasma treatment for 1 h and prestretching of 40%, the wrinkled 3D foam greatly improves specific surface area and stretchability by over 60% and 75%, respectively, compared with the pristine 3D PDMS foam. To prove its applicability with improved performances, supercapacitors are prepared by coating a conductive material on the wrinkled 3D foam. The resulting supercapacitors exhibit an increased storage capacity (8.3 times larger), maintaining storage capacity well under stretching up to 50%.

KEYWORDS: 3D foam, wrinkles, polymeric foam, nanostructures, supercapacitor



INTRODUCTION

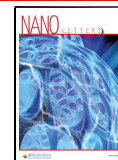
Three-dimensional (3D) porous foam, which is remarkably different from bulk structures, has attracted much interest because of its improved total surface area for reaction with chemicals and mechanical deformability to be stretchable and compressible, which further extends its application capabilities to flexible conductors, energy harvesting and storage, sensors, absorbents and separators, and biomedical devices.^{1–5} Compared with the most commonly reported 3D porous foams in which conductive materials (e.g., graphene and carbon nanotubes) are interconnected in a hierarchical formation,^{6–12} 3D polymeric foams comprising polymers such as polydimethylsiloxane (PDMS)^{13–16} have a great advantage owing to their mechanical and chemical robustness. As a result, they are believed to provide a facile and industrial approach to various application fields such as supercapacitors, stretchable conductors, and sensors,^{16–20} by coating conductive materials on the surface of polymers. However, there is still a strong requirement to further enhance the surface area and stretchability for their use in the related applications. Although some efforts such as regulation of pore size, pore geometry, pore distribution, and closed/open porous frameworks^{11,21–24} have been proposed to satisfy the requirements, they need relatively complicated processes for facile fabrication and have limitations in controlling the surface architecture of porous foams.

Implementing a wrinkled structure on the underlying surface of 3D polymeric foams has been recognized as one of the most promising strategies to increase not only the surface area due to the increased trajectory length per unit area by surface bends, but also stretchability due to the existence of a stretch-release region under tensile strain.^{25–27} Much effort has been made to generate controlled wrinkles on two-dimensional (2D) surfaces.^{28–31} Tiny wrinkles are spontaneously formed by a mismatch between the elastic properties of neighboring layers with sequential expansion and contraction in a multilayered system with strong dependency on film thickness and strain for wavelength and amplitude. Highly ordered wrinkles have mainly been formed by relaxation of compliant substrates that are mechanically and thermally pre-stretched.^{32–38} Surface treatment with UV ozone or oxygen plasma to form a stiff layer on homogeneous material can also produce a wrinkled structure.³⁹ Although efforts have been made to create wrinkles on 2D films, they have seldom been reported to create tiny wrinkles on 3D architectures. The precisely controlled wrinkled architectures in polymeric three-

Received: April 8, 2021

Revised: June 17, 2021

Published: June 22, 2021



dimensional form structures were considered challenging and very promising for application in a variety of deformable electric and energy devices.

Here, we report a facile strategy to simultaneously enhance the surface area and stretchability of 3D polymeric foams. The wrinkling structure is tailored to the 2D strut surfaces inside the 3D PDMS polymeric foam by introducing a plasma treatment method on prestretched 3D PDMS foam followed by relaxation. The wrinkles are easily controlled by regulating the plasma treatment time and applied prestrain. The wrinkled 3D foam (plasma treatment of 1 h and prestretching of 40%) exhibited improvements in both the specific surface area (SSA) by over 60% and stretchability by over 75% compared with the pristine 3D foam. Using the wrinkled 3D foam with conductive coating, we finally demonstrate a highly stretchable supercapacitor that exhibits improved performance with not only increased volumetric capacitance but also excellent stretching-tolerance capability.

RESULTS AND DISCUSSION

Fabrication of Wrinkled 3D PDMS Foam. The preparation process for obtaining the wrinkled 3D PDMS foam is illustrated in Figure 1a (for details, see Supporting

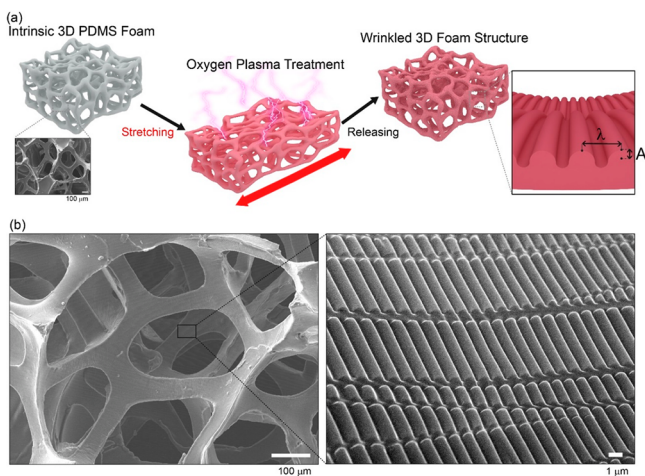


Figure 1. Generation of wrinkled 3D PDMS foam. (a) Schematic of the fabrication process for generating a wrinkle structure in intrinsic 3D PDMS foam. Wrinkles were formed on the surface layer of PDMS struts by developing SiO_x-PDMS bilayer with plasma vitrification on prestretched intrinsic 3D PDMS foam. Wavelength (λ) and amplitude (A) of wrinkles are defined as the distance between adjacent peaks and the half distance between a peak, respectively. (b) SEM images of representative wrinkling pattern obtained by prestrain of 40% followed by releasing process and oxygen plasma exposure for 1 h.

Information (SI) Experimental Section and Figure S1). First, the 3D PDMS foam was prepared by coating a diluted PDMS solution (PDMS of 10 wt % with ethyl acetate) on an interconnected 3D scaffold of rigid nickel metal using a dip-coating method, followed by removal of the nickel using FeCl₃ etchant.¹⁶ To form wrinkles on the surface of struts in the PDMS foam, the foam was uniaxially stretched with a tensile strain. An oxygen plasma was then used to harden the strut surfaces of PDMS forming bilayer PDMS, in which the surface layer (oxidized PDMS, SiO_x) is harder than the inner layer (pristine PDMS, [SiO(CH₃)₂]_n) due to cleavage of Si-CH₃ groups.³⁶ With a mechanical release, wrinkles were generated on the surface layer of the PDMS struts. Note that the wrinkles

cannot be created using only the oxygen plasma treatment or mechanical stretching-releasing process (SI Figure S2). For this wrinkling architecture, we defined the wavelength (λ) as the distance between adjacent peaks or troughs and the amplitude (A) as the half-distance between a peak and a trough. Figure 1b shows the scanning electron microscopy (SEM) image of the hierarchical wrinkling structure in the 3D PDMS foam. The controlled microscopic wrinkles were distributed on all of the struts of the foam (SI Figure S3). Although uniaxial tensile strain was applied to the intrinsic PDMS foam, the spatial arrangement in the strain direction due to the softness of PDMS and the 3D structural flexibility induces the applied mechanical strain on all strut surfaces, thus forming wrinkles on the engaging surface of the PDMS foam. In-plane trough lines perpendicular to wrinkle patterns (SI Figure S4) are caused since the oxidized layer is expanded in a direction perpendicular to the tensile direction due to the Poisson effect of elastic PDMS struts.

Strain Distribution in the 3D PDMS Foam. The strain distribution on the struts inside the 3D PDMS foam due to the mechanically applied uniaxial tensile strain is shown in Figure 2. Finite element analysis (FEA) using COMSOL Multiphysics software was performed based on an X-ray microcomputed tomography (micro-CT) image obtained by scanning the 3D foam (SI Figure S5). To apply the uniaxial tensile strain to the computed model, the displacement of one side of the 3D foam was prescribed with a fixed opposite side. As shown in Figure 2a, the applied strain drove both the arrangement of the 3D interconnected polygonal struts in the direction of the applied strain with structural deformation as well as the direct stretching of struts in the 3D foam. It should be noted that the initial tensile strain was redistributed in the porous structure depending on the thickness of the local strut. The strain was more localized on the narrow region of the porous strut than the thicker region. We focus on identifying the local strain within both regions and calculate it by computing the slope of the line in Figure 2c. In the case of struts crossing the pore (Figure 2c), the local strain can be expressed as follows

$$\varepsilon_m = 1.63\varepsilon_{pre} \pm 0.26 \quad (1)$$

where ε_{pre} is the prestrain to stretch the 3D foam and ε_m is the modified strain localized and concentrated to the struts. The results indicate that a strain larger than the prestrain condition was applied, particularly in the narrow region during the oxygen plasma treatment and mechanical stretching-releasing process. Considering that wrinkles are formed under the prestretched condition, the wrinkled structure actually formed under high stresses, which were induced by a strain larger than the applied prestrain. We also compared the stress distribution of inner (about 600 μ m from the surface) and outer (surface) struts of the 3D foam through FEA when stretching (SI Figure S6). Larger strains than the prestrain were induced to both of the inner and outer struts. We performed the quantification based on the wrinkles inside the 3D foam.

Controlled Wrinkle Formation in 3D PDMS Foam. The controllability of the wrinkling structure on the strut surfaces inside the 3D foam is shown in Figure 3. Considering the modified strain ($\varepsilon_m = 1.63\varepsilon_{pre}$) applied to the surface of the 3D foam owing to the applied prestrain (ε_{pre}), the wavelength (λ), and the amplitude (A) of the wrinkles can be expressed as follows^{34,40,41}

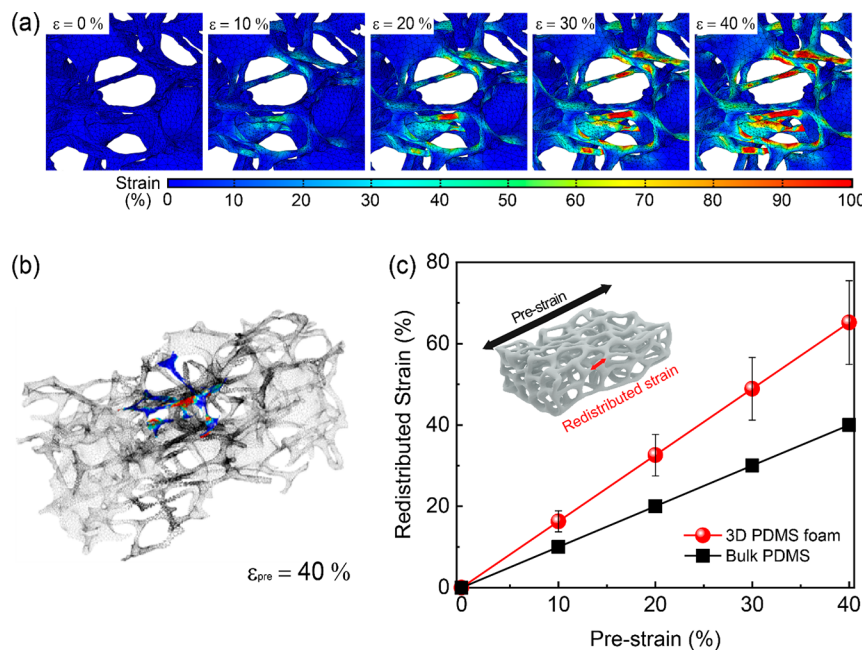


Figure 2. Strain distribution on the strut surface inside the 3D PDMS foam applied uniaxial tensile strain. (a) Successive FEA simulation of the strain distribution under stretching up to 40%. (b) Numerically measured points for redistributed strain on the strut surface. (c) Redistributed strain on the strut surface versus prestrain applied to the 3D PDMS foam. The measured redistributed strain is the average value of several elements in the narrow section of the strut. The resulting graph for bulk PDMS is offered as a reference.

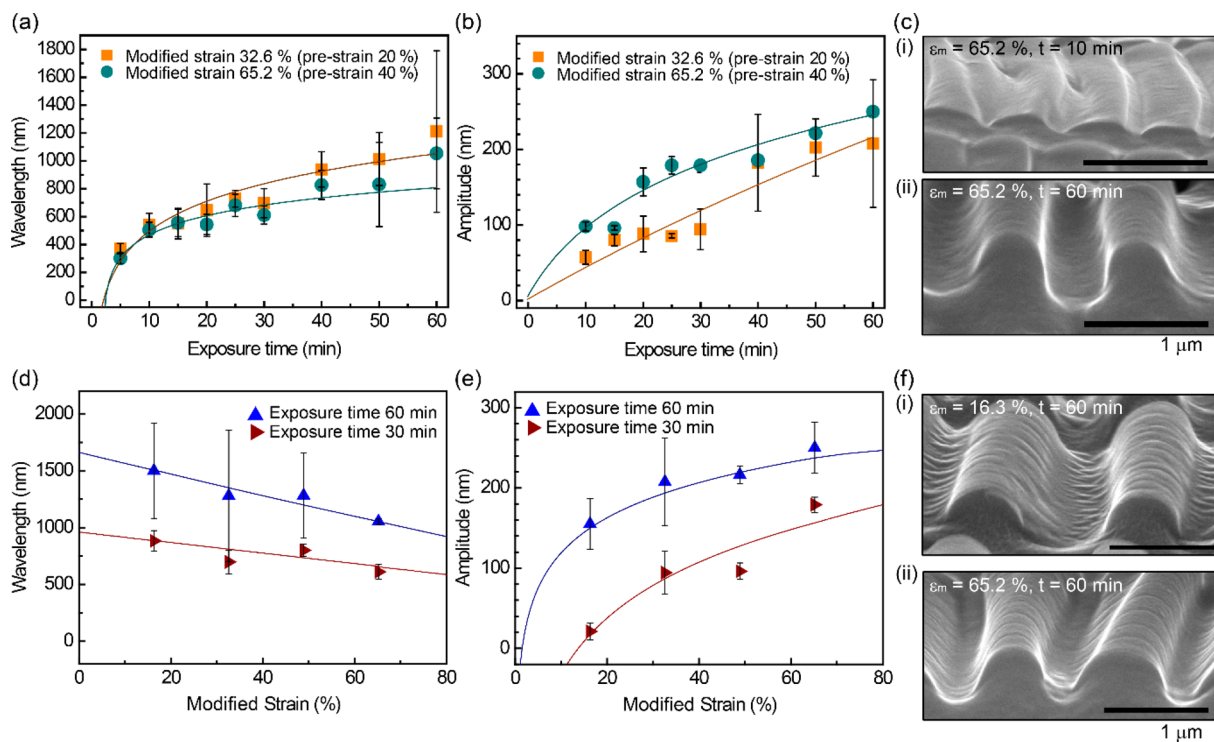


Figure 3. Controllability of wrinkles on the strut surfaces in the 3D PDMS foam. (a) Wavelength and (b) amplitude of wrinkles dependent on exposure time of oxygen plasma that decides the thickness (h) of the surface layer that is hardened. (c) SEM images of wrinkles generated after treatment of oxygen plasma for 10 and 60 min. The same modified strain ($\epsilon_m = 65.2\%$) was applied. (d) Wavelength and (e) amplitude of wrinkles dependent on modified strain. (f) SEM images of wrinkles generated after treatment of mechanically modified strain of 16.3% and 65.2%. The same exposure time of oxygen plasma treatment (10 min) was applied.

$$\lambda = \frac{2\pi h}{(1 + \epsilon_m)\left(1 + \frac{s}{32}\epsilon_m(1 + \epsilon_m)\right)^{1/3} \left(\frac{\bar{E}_s}{3\bar{E}_i}\right)^{1/3}} \quad (2)$$

$$A = \frac{h}{\sqrt{(1 + \epsilon_m)\left(1 + \frac{s}{32}\epsilon_m(1 + \epsilon_m)\right)^{1/3}}} \sqrt{\frac{\epsilon_m}{\epsilon_c} - 1} \quad (3)$$

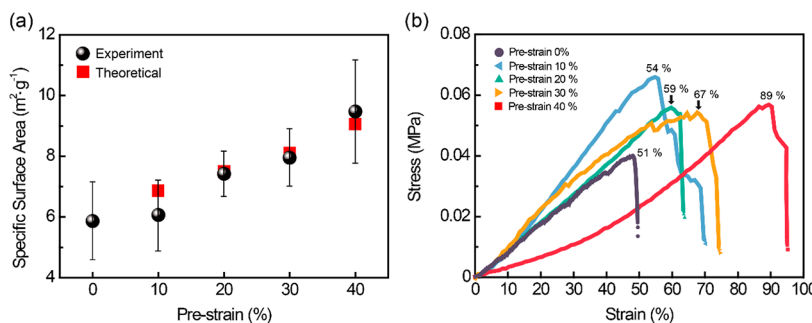


Figure 4. Properties of the wrinkled 3D PDMS foam. (a) Specific surface area according to the applied prestrain. For reference, the theoretical modeling was conducted by calculating the ideal length of trajectory due to the wavy architectures of wrinkles. (b) Stress–strain curves with different prestrains.

$$\epsilon_c = \frac{1}{4} \left(\frac{3\bar{E}_i}{E_s} \right)^{2/3} \quad (4)$$

where \bar{E} is the plane-strain modulus, calculated as $\bar{E} = E/(1 - \nu^2)$; E is the Young's modulus; ν is the Poisson ratio; h is the thickness of the glassy surface layer; and ϵ_c is the strain when wrinkling structures start to be generated on the struts. The subscripts s and i refer to the glassy surface layer and pristine inner layer of the struts, respectively. Figure 3a,b shows the wavelength and amplitude of wrinkles, respectively, with increasing exposure time of oxygen plasma, which determines the penetration depth of oxide links from the PDMS surface, thus determining the thickness of the surface layer that is hardened. It is well-known that the penetration depth for the thickness (h) of the oxidized layer exhibits a logarithmic dependence on the O_2 plasma exposure time.^{36,42} Such dependence is described by the chemical kinetics of the spatiotemporal conversion reaction in which methyl groups are substituted with hydroxyl groups and then oxide links occur. Consequently, the logarithmic dependence of the thickness (h) of the surface layer in 3D foam can be described in accordance with the previous frontal glassy layer-formation model^{36,42}

$$h = \frac{\ln(p \times t)}{\mu} - \frac{1}{\mu} \ln \left(\frac{1}{KI_0} \ln \left(\frac{1}{1 - \Phi_c} \right) \right) \quad (5)$$

where t is the plasma exposure time, μ is the material attenuation coefficient by hindering and depleting ionic and radical oxygen, p is the power applied in the plasma chamber, K is the overall reaction rate constant, I_0 is the plasma intensity at the top surface of the strut, and Φ_c is the threshold of a PDMS conversion proportion Φ required to form a sufficiently hard oxidized layer for wrinkling. Prestrains of 20% and 40% corresponding to the modified strains of 32.6% and 65.2%, respectively, were applied to create wrinkles. Because the wavelength and amplitude of wrinkles generally show a linear dependence on the thickness (h) of the hardened layer, the logarithmic relations in wavelength and amplitude according to exposure time are very reasonable results. Moreover, such results are clearly seen in the SEM images in Figure 3c, in which the PDMS surfaces of 3D foam were treated with oxygen plasma for 10 and 60 min to form a different thickness of the hardened layer. Similarly, we obtained the wavelength and amplitude of wrinkles with increasing modified strains induced by uniaxially applied prestrain, as shown in Figure 3d,e. The results indicate that the wavelength is inversely proportional to the applied strain, and the amplitude has a

logarithmic relationship. Higher strain shows shorter wavelength and higher amplitude, as shown in Figure 3f. In particular, the wavelength and amplitude of the hierarchical wrinkles formed on the strut surfaces in the 3D foam exhibit the same mechanics as those generated on 2D surfaces, thus enabling wrinkles in a 3D structure using the known wrinkle generation mechanism.^{34,42}

Properties of Wrinkled 3D PDMS Foam. Improvement of performances such as surface area and stretchability owing to wrinkles in the 3D PDMS foam was confirmed, as illustrated in Figure 4. First, the SSA of the 3D foam samples was measured based on X-ray micro-CT.⁴³ The prestrains (10%, 20%, 30%, and 40% corresponding to modified strains of 16.3%, 32.6%, 48.9%, and 65.2%, respectively) were applied to create wrinkles with different wavelengths and amplitudes that resulted in differences in the total surface area per volume, while the plasma treatment time was 1 h. Theoretical modeling was also conducted to compare the results with experimental values. The modeling results were obtained by calculating the ideal length of the trajectory due to the wavy architectures of wrinkles. Figure 4a shows the SSA depending on the prestrain, both experimentally and theoretically. As the prestrain increases, the SSA increases owing to an increase in the total length of the trajectory due to the amplitude. In addition, the experimental results match well with the theoretical results, as shown in Figure 4a. With prestrains of 10%, 20%, and 30%, the experimental results of SSA are slightly lower than the theoretically predicted values because the prestrain applied at the low tensile strain was used to spatially arrange the struts in the direction of the applied strain. Meanwhile, the wrinkled 3D foam with a prestrain of 40% characterizes a higher SSA value than the theoretical one. This is because additional surface structures occur apart from wrinkle architectures on the PDMS surface owing to the stretching–releasing operation over the mechanical threshold (SI Figure S7), and wrinkles are formed on almost all the struts in the 3D foam due to high strain (SI Figure S3). In particular, the wrinkled 3D foam with prestrain 40% and plasma treatment for 1 h exhibited an SSA improvement of 60% over the intrinsic 3D foam owing to the wrinkles. This SSA improvement is, in fact, the main purpose for generating the 3D foam structure beyond the bulk structure and can play a critical role in potential applications such as chemical reactions, oil absorption, supercapacitors, and energy harvesting systems.

To confirm the enhancement of mechanical stretchability due to the wrinkling structure in the 3D foam, we conducted strain–stress curve measurements, as shown in Figure 4b. An increase in prestrain enhances the total length of the trajectory

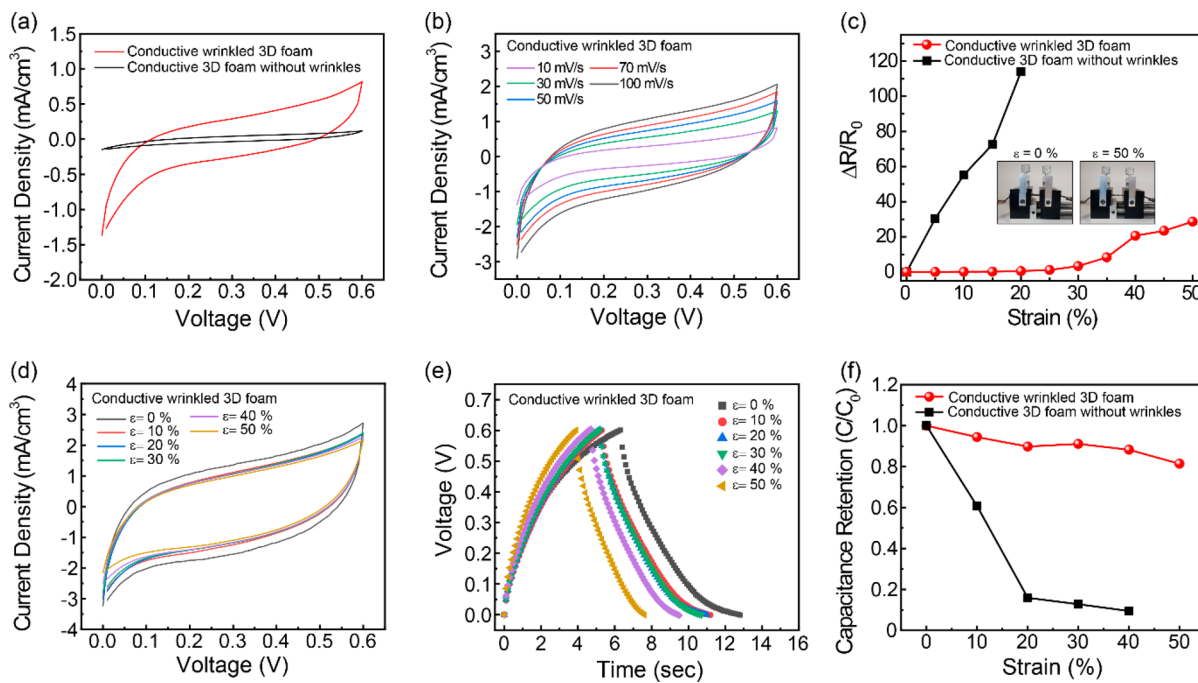


Figure 5. Wrinkled 3D foam electrodes for high-performance supercapacitors. (a) Comparison of CV curves of the wrinkled 3D foam electrode and the 3D foam electrode without wrinkles. The scan rate is 10 mV/s. (b) CV curves of the conductive wrinkled 3D foam supercapacitor with scan rates of 10–100 mV/s. (c) Normalized change in electrical resistance of the 3D foam electrodes under stretching. (d) CV curves measured with increasing strain in the tensile direction with tensile strains ranging from 0% to 50% for the conductive wrinkled 3D foam supercapacitor with the same scan rate of 100 mV/s. (e) Galvanostatic charge–discharge curves of the wrinkled 3D foam electrode measured with tensile strains from 0% to 50%. The current density is 2 mA/cm². (f) Capacitance retention versus strain of the 3D foam electrodes during each stretching–releasing cycle at the same scan rate of 100 mV/s. For the conductive wrinkled 3D foam, the wrinkled 3D PDMS foam with prestrain 40% and plasma exposure for 1 h is applied to all graphs.

by increasing the amplitude, and as a result, the mechanical stretchability increases. The wrinkled 3D PDMS foam with a prestrain of 40% had a stretchability of 89%, indicating ~75% reinforcement compared to the pristine 3D PDMS foam. Furthermore, the wrinkled foam with prestrain 40% and plasma treatment for 1 h showed the elastic modulus of 0.1 MPa, the tensile strength of 0.057 MPa, and the maximum stretchability more than 85% even after 100 stretching–releasing cycles of 80% strain (SI Figure S8). As a result, the formation of wrinkles in the 3D foam structure enables a foam device to perform its unique function even under external strain.

Wrinkled 3D Foam Electrodes for High-Performance Supercapacitors. A remarkable advantage of the wrinkled 3D foam is that it can serve as an effective electrode with a simple conductive coating to form a highly stretchable electrochemical energy storage system with enhanced storage capability. To demonstrate highly elastic supercapacitors, we coated a conductive material onto the wrinkled 3D PDMS foam with prestrain 40% and plasma for 1 h (SI Figure S9). Cyclic voltammetry (CV) curves were obtained for the conductive wrinkled 3D foam and the intrinsic 3D foam electrode without wrinkles, as shown in Figure 5a. Although the intrinsic 3D foam electrode can be an electrochemical double-layer capacitor, the specific capacitance could be dramatically increased such that approximately 8.3 times larger CV curves were obtained owing to the increase in the surface area with an internal wrinkling structure in the 3D foam. In addition, we demonstrated that the increase in the prestrain applied when the wrinkled 3D foam is created affects the enhancement of the specific capacitance as shown in SI Figure S10. This tendency

is consistent with the result of the increase in SSA depending on the prestrain. The CV curves measured with scan rates of 10–100 mV/s are presented in Figure 5b and SI Figure S11. Furthermore, the energy storage capability can be dramatically improved by coating a well-known pseudocapacitive MnO₂,⁴⁴ which is abundant and environmentally friendly and has a high theoretical specific capacitance (SI Figure S12). An investigation of the effects of mechanical deformation by tensile strain on the electrochemical performances of the wrinkled 3D foam supercapacitor was conducted. Although a metal electrode with low stretching-resistance was used, the wrinkled 3D foam supercapacitor exhibited low resistance change, even up to strain of 50% (Figure 5c). In addition, the CV values could be measured under application of static tensile strain in Figure 5d and SI Figure S13. Triangular galvanostatic charge–discharge curves and Nyquist curves of the wrinkled 3D foam electrode with increasing strain were investigated as shown in Figure 5e and SI Figure S14, respectively. After stretching until 50%, the charge and discharge time were almost retained without major delays. By defining capacitance retention (C/C_0) as the rate of capacitance after stretching to the initial capacitor (Figure 5f), negligible changes were observed in the CV values when the strain applied varied from 0% to 50% in the tensile direction. Approximately 81% of the capacitance of the wrinkled 3D foam supercapacitor was retained at 50% strain application, whereas the intrinsic 3D foam-based supercapacitor lost conductivity at 20% strain, and the capacitance capability dramatically decreased after strain was applied. Also, the wrinkled foam electrode showed stable electrochemical performance during 50% stretching/releasing cycles as shown in SI Figure S15. After 100 stretching/

releasing cycles, the wrinkled foam electrode has retained about 95% of its capacitance since the wrinkling structure in the 3D foam electrode absorbed the mechanical deformation. These results prove that our approach of incorporating wrinkle structures in a 3D foam is a very effective method for supercapacitors to achieve a highly stretchable and high-capacitor capacity.

CONCLUSION

We present a facile strategy to generate controlled wrinkles in 3D architectures for high surface area and stretchability. In the 3D PDMS polymeric foam, wrinkles occur on the 2D strut surfaces because the hard layer is formed via plasma treatment on the prestretched soft PDMS surfaces followed by relaxation. The wrinkles in the 3D foam can be structurally adjusted by the plasma treatment time and applied prestrain. Because of the increase in the trajectory length per unit area of the wrinkles, the wrinkled 3D foam not only increased the surface area but also enhanced stretchability in comparison with the existing pristine 3D foam. For practical applications of the wrinkled 3D foam, high-capacity and high-stretchability supercapacitors were fabricated by coating a conductive material onto wrinkled surfaces. Consequently, it was demonstrated that wrinkled structures enhance the storage capacity of the supercapacitors as well as provide great strain tolerance. Introducing controllable wrinkles in 3D polymeric foam can overcome the limitations of conventional bulk and 3D porous foams by improving the surface area and stretchability concurrently. High-performance wrinkled 3D polymeric foams are expected to pave the way for potential applications such as stretchable conductors, energy harvesting and storage, sensors, absorbents and separators, and biomedical devices.

ASSOCIATED CONTENT

Supporting Information

The Supporting Information is available free of charge at <https://pubs.acs.org/doi/10.1021/acs.nanolett.1c01384>.

Experimental section, fabrication of 3D PDMS foam; SEM images of wrinkled 3D foam; X-ray micro-computed tomography images of the 3D PDMS foam; analysis on tensile stress distribution on outer and inner struts of the 3D PDMS foam based on FEA simulation; electrochemical properties of the conductive wrinkled 3D foam electrodes and the conductive 3D foam without wrinkles ([PDF](#))

AUTHOR INFORMATION

Corresponding Authors

Sungwoo Chun — Department of Electronics and Information Engineering, Korea University, Sejong 30019, Republic of Korea; Email: swchun127129@korea.ac.kr

Changhyun Pang — School of Chemical Engineering, Sungkyunkwan University (SKKU), Jangan-gu, Suwon 16419, Republic of Korea; orcid.org/0000-0001-8339-7880; Email: chpang@skku.edu

Authors

Siyeon Jang — School of Chemical Engineering, Sungkyunkwan University (SKKU), Jangan-gu, Suwon 16419, Republic of Korea

Hyeongho Min — SKKU Advanced Institute of Nanotechnology, Sungkyunkwan University (SKKU), Jangan-gu, Suwon 16419, Republic of Korea

Sung Beom Cho — Virtual Engineering Center, Korea Institute of Ceramic Engineering and Technology (KICET), Jinju-si, Gyeongsangnam-do 52851, Republic of Korea

Hyeon Woo Kim — Virtual Engineering Center, Korea Institute of Ceramic Engineering and Technology (KICET), Jinju-si, Gyeonsangnam-do 52851, Republic of Korea

Wonkyeong Son — Department of Energy and Materials Engineering, Dongguk University-Seoul, Seoul 04620, Republic of Korea

Changsoon Choi — Department of Energy and Materials Engineering, Dongguk University-Seoul, Seoul 04620, Republic of Korea; orcid.org/0000-0003-4456-4548

Complete contact information is available at: <https://pubs.acs.org/10.1021/acs.nanolett.1c01384>

Author Contributions

The manuscript was written through contributions of all authors. All authors have given approval to the final version of the manuscript.

Notes

The authors declare no competing financial interest.

ACKNOWLEDGMENTS

We gratefully acknowledge support from the Korea Institute of Industrial Technology as “Development of smart textronic products based on electronic fibers and textiles” (kitech JA-21-0001). This study was conducted with the support of the Gyeongi-Do Technology Development Program as “Development of smart textronic products based on electronic fibers and textiles (kitech IZ-21-0001)”. This research was supported by Basic Science Research Program through the National Research Foundation of Korea (NRF) funded by the Ministry of Education (2014R1A6A1030732 and 2019R1C1C1008730).

REFERENCES

- (1) Choi, H. W.; Jeong, D. I.; Woo, S.; Kwon, S. B.; Wu, S.; Kim, J. H.; Yang, W. S.; Kang, B. K.; Lim, B.; Yoon, D. H. Morphology Adjustable Coax With 3D Mesoporous Structure And Amorphous N-Doped Carbon For Overall Water Splitting. *Appl. Surf. Sci.* **2020**, *529*, 147177.
- (2) Ji, F.; Wang, L.; Yang, J.; Wu, X.; Li, M.; Jiang, S.; Lin, S.; Chen, Z. Highly Compact, Free-Standing Porous Electrodes From Polymer-Derived Nanoporous Carbons For Efficient Electrochemical Capacitive Deionization. *J. Mater. Chem. A* **2019**, *7* (4), 1768–1778.
- (3) Slater, A. G.; Cooper, A. I. Function-Led Design Of New Porous Materials. *Science* **2015**, *348* (6238), aaa8075.
- (4) Wu, D.; Xu, F.; Sun, B.; Fu, R.; He, H.; Matyjaszewski, K. Design And Preparation Of Porous Polymers. *Chem. Rev.* **2012**, *112* (7), 3959–4015.
- (5) Yang, X.-Y.; Chen, L.-H.; Li, Y.; Rooke, J. C.; Sanchez, C.; Su, B.-L. Hierarchically Porous Materials: Synthesis Strategies And Structure Design. *Chem. Soc. Rev.* **2017**, *46* (2), 481–558.
- (6) Chen, K.; Shi, L.; Zhang, Y.; Liu, Z. Scalable Chemical-Vapour-Deposition Growth Of Three-Dimensional Graphene Materials Towards Energy-Related Applications. *Chem. Soc. Rev.* **2018**, *47* (9), 3018–3036.
- (7) Paul, R.; Etacheri, V.; Pol, V. G.; Hu, J.; Fisher, T. S. Highly Porous Three-Dimensional Carbon Nanotube Foam As A Free-standing Anode For A Lithium-Ion Battery. *RSC Adv.* **2016**, *6* (83), 79734–79744.

- (8) Wu, L.; Li, W.; Li, P.; Liao, S.; Qiu, S.; Chen, M.; Guo, Y.; Li, Q.; Zhu, C.; Liu, L. Powder, Paper And Foam Of Few-Layer Graphene Prepared In High Yield By Electrochemical Intercalation Exfoliation Of Expanded Graphite. *Small* **2014**, *10* (7), 1421–1429.
- (9) Yeo, S. J.; Oh, M. J.; Yoo, P. J. Structurally Controlled Cellular Architectures For High-Performance Ultra-Lightweight Materials. *Adv. Mater.* **2019**, *31* (34), 1803670.
- (10) Feng, D.; Lei, T.; Lukatskaya, M. R.; Park, J.; Huang, Z.; Lee, M.; Shaw, L.; Chen, S.; Yakovenko, A. A.; Kulkarni, A.; Xiao, J.; Fredrickson, K.; Tok, J. B.; Zou, X.; Cui, Y.; Bao, Z. Robust And Conductive Two-Dimensional Metal–Organic Frameworks With Exceptionally High Volumetric And Areal Capacitance. *Nat. Energy* **2018**, *3* (1), 30–36.
- (11) Maiti, U. N.; Lim, J.; Lee, K. E.; Lee, W. J.; Kim, S. O. Three-Dimensional Shape Engineered, Interfacial Gelation Of Reduced Graphene Oxide For High Rate, Large Capacity Supercapacitors. *Adv. Mater.* **2014**, *26* (4), 615–619.
- (12) Salunkhe, R. R.; Kaneti, Y. V.; Kim, J.; Kim, J. H.; Yamauchi, Y. Nanoarchitectures For Metal–Organic Framework-Derived Nanoporous Carbons Toward Supercapacitor Applications. *Acc. Chem. Res.* **2016**, *49* (12), 2796–2806.
- (13) Chen, Q.; Zhao, J.; Ren, J.; Rong, L.; Cao, P. F.; Advincula, R. C. 3D Printed Multifunctional, Hyperelastic Silicone Rubber Foam. *Adv. Funct. Mater.* **2019**, *29* (23), 1900469.
- (14) Chen, Z.; Ren, W.; Gao, L.; Liu, B.; Pei, S.; Cheng, H.-M. Three-Dimensional Flexible And Conductive Interconnected Graphene Networks Grown By Chemical Vapour Deposition. *Nat. Mater.* **2011**, *10* (6), 424–428.
- (15) Fu, Y.; Xu, F.; Weng, D.; Li, X.; Li, Y.; Sun, J. Superhydrophobic Foams With Chemical-And Mechanical-Damage-Healing Abilities Enabled By Self-Healing Polymers. *ACS Appl. Mater. Interfaces* **2019**, *11* (40), 37285–37294.
- (16) Zhu, D.; Handschuh-Wang, S.; Zhou, X. Recent Progress In Fabrication And Application Of Polydimethylsiloxane Sponges. *J. Mater. Chem. A* **2017**, *5* (32), 16467–16497.
- (17) Chen, M.; Zhang, L.; Duan, S.; Jing, S.; Jiang, H.; Li, C. Highly Stretchable Conductors Integrated With A Conductive Carbon Nanotube/Graphene Network And 3D Porous Poly (Dimethylsiloxane). *Adv. Funct. Mater.* **2014**, *24* (47), 7548–7556.
- (18) Chen, Z.; Xu, C.; Ma, C.; Ren, W.; Cheng, H. M. Lightweight And Flexible Graphene Foam Composites For High-Performance Electromagnetic Interference Shielding. *Adv. Mater.* **2013**, *25* (9), 1296–1300.
- (19) Jia, J.; Sun, X.; Lin, X.; Shen, X.; Mai, Y.-W.; Kim, J.-K. Exceptional Electrical Conductivity And Fracture Resistance Of 3D Interconnected Graphene Foam/Epoxy Composites. *ACS Nano* **2014**, *8* (6), 5774–5783.
- (20) Zhou, G.; Li, L.; Ma, C.; Wang, S.; Shi, Y.; Koratkar, N.; Ren, W.; Li, F.; Cheng, H.-M. A Graphene Foam Electrode With High Sulfur Loading For Flexible And High Energy Li-S Batteries. *Nano Energy* **2015**, *11*, 356–365.
- (21) Chen, G.; Rastak, R.; Wang, Y.; Yan, H.; Feig, V.; Liu, Y.; Jiang, Y.; Chen, S.; Lian, F.; Molina-Lopez, F.; Jin, L.; Cui, K.; Chung, J. W.; Pop, E.; Linder, C.; Bao, Z. Strain-And Strain-Rate-Invariant Conductance In A Stretchable And Compressible 3D Conducting Polymer Foam. *Matter* **2019**, *1* (1), 205–218.
- (22) Deng, W.; Fang, Q.; Zhou, X.; Cao, H.; Liu, Z. Hydrothermal Self-Assembly Of Graphene Foams With Controllable Pore Size. *RSC Adv.* **2016**, *6* (25), 20843–20849.
- (23) Miao, F.; Lu, N.; Zhang, P.; Zhang, Z.; Shao, G. Multi-dimension-Controllable Synthesis Of Ant Nest-Structural Electrode Materials With Unique 3D Hierarchical Porous Features Toward Electrochemical Applications. *Adv. Funct. Mater.* **2019**, *29* (29), 1808994.
- (24) Xiao, M.; Kong, T.; Wang, W.; Song, Q.; Zhang, D.; Ma, Q.; Cheng, G. Interconnected Graphene Networks With Uniform Geometry For Flexible Conductors. *Adv. Funct. Mater.* **2015**, *25* (39), 6165–6172.
- (25) Li, B.; Cao, Y.-P.; Feng, X.-Q.; Gao, H. Mechanics Of Morphological Instabilities And Surface Wrinkling In Soft Materials: A Review. *Soft Matter* **2012**, *8* (21), 5728–5745.
- (26) Rodriguez-Hernandez, J. Wrinkled Interfaces: Taking Advantage Of Surface Instabilities To Pattern Polymer Surfaces. *Prog. Polym. Sci.* **2015**, *42*, 1–41.
- (27) An, T.; Cheng, W. Recent Progress In Stretchable Supercapacitors. *J. Mater. Chem. A* **2018**, *6* (32), 15478–15494.
- (28) Chen, C. M.; Yang, S. Wrinkling Instabilities In Polymer Films And Their Applications. *Polym. Int.* **2012**, *61* (7), 1041–1047.
- (29) Cheng, X.; Miao, L.; Su, Z.; Chen, H.; Song, Y.; Chen, X.; Zhang, H. Characterization Of Forced Localization Of Disordered Weakly Coupled Micromechanical Resonators. *Microsyst. Nanoeng.* **2017**, *3* (1), 1–9.
- (30) Li, T.; Hu, K.; Ma, X.; Zhang, W.; Yin, J.; Jiang, X. Hierarchical 3D Patterns With Dynamic Wrinkles Produced By A Photocontrolled Diels–Alder Reaction On The Surface. *Adv. Mater.* **2020**, *32* (7), 1906712.
- (31) Yu, S.; Ma, L.; Sun, Y.; Lu, C.; Zhou, H.; Ni, Y. Controlled Wrinkling Patterns In Periodic Thickness-Gradient Films On Polydimethylsiloxane Substrates. *Langmuir* **2019**, *35* (22), 7146–7154.
- (32) Bowden, N.; Brittain, S.; Evans, A. G.; Hutchinson, J. W.; Whitesides, G. M. Spontaneous Formation Of Ordered Structures In Thin Films Of Metals Supported On An Elastomeric Polymer. *Nature* **1998**, *393* (6681), 146–149.
- (33) Chung, S.; Lee, J. H.; Moon, M. W.; Han, J.; Kamm, R. D. Non-Lithographic Wrinkle Nanochannels For Protein Preconcentration. *Adv. Mater.* **2008**, *20* (16), 3011–3016.
- (34) Jiang, H.; Khang, D.-Y.; Song, J.; Sun, Y.; Huang, Y.; Rogers, J. A. Finite Deformation Mechanics In Buckled Thin Films On Compliant Supports. *Proc. Natl. Acad. Sci. U. S. A.* **2007**, *104* (40), 15607–15612.
- (35) Nagashima, S.; Ebrahimi, H.; Lee, K. R.; Vaziri, A.; Moon, M. W. Tunable Nanochannels Fabricated By Mechanical Wrinkling/Folding Of A Stiff Skin On A Soft Polymer. *Adv. Mater. Interfaces* **2015**, *2* (3), 1400493.
- (36) Nania, M.; Matar, O. K.; Cabral, J. T. Frontal Vitrification Of PDMS Using Air Plasma And Consequences For Surface Wrinkling. *Soft Matter* **2015**, *11* (15), 3067–3075.
- (37) Okayasu, T.; Zhang, H. L.; Bucknall, D. G.; Briggs, G. A. D. Spontaneous Formation Of Ordered Lateral Patterns In Polymer Thin-Film Structures. *Adv. Funct. Mater.* **2004**, *14* (11), 1081–1088.
- (38) Uchida, N.; Ohzono, T. Orientational Ordering Of Buckling-Induced Microwrinkles On Soft Substrates. *Soft Matter* **2010**, *6* (22), 5729–5735.
- (39) Yang, S.; Khare, K.; Lin, P. C. Harnessing Surface Wrinkle Patterns In Soft Matter. *Adv. Funct. Mater.* **2010**, *20* (16), 2550–2564.
- (40) Huang, R. Kinetic Wrinkling Of An Elastic Film On A Viscoelastic Substrate. *J. Mech. Phys. Solids* **2005**, *53* (1), 63–89.
- (41) Huang, Z.; Hong, W.; Suo, Z. Nonlinear Analyses Of Wrinkles In A Film Bonded To A Compliant Substrate. *J. Mech. Phys. Solids* **2005**, *53* (9), 2101–2118.
- (42) Bayley, F. A.; Liao, J. L.; Stavrinou, P. N.; Chiche, A.; Cabral, J. T. Wavefront Kinetics Of Plasma Oxidation Of Polydimethylsiloxane: Limits For Sub- μm Wrinkling. *Soft Matter* **2014**, *10* (8), 1155–1166.
- (43) Yu, C.; Yu, C.; Cui, L.; Song, Z.; Zhao, X.; Ma, Y.; Jiang, L. Facile Preparation Of The Porous PDMS Oil-Absorbent For Oil/Water Separation. *Adv. Mater. Interfaces* **2017**, *4* (3), 1600862.
- (44) Choi, C.; Kim, J. H.; Sim, H. J.; Di, J.; Baughman, R. H.; Kim, S. J. Microscopically Buckled And Macroscopically Coiled Fibers For Ultra-Stretchable Supercapacitors. *Adv. Energy Mater.* **2017**, *7* (6), 1602021.